Original paper

Immune-associated renal disease found in caspase 3-deficient mice

Takashi Suzuki[1#], Osamu Ichii[1*#], Teppei Nakamura[1,2], Taro Horino[3], Yaser Hosny Ali Elewa[1,4] & Yasuhiro Kon[1]

#: these authors are equally contributed.

Names, addresses, and email IDs of authors:

1. Laboratory of Anatomy, Department of Basic Veterinary Sciences, Faculty of Veterinary Medicine, Hokkaido University, Sapporo, Japan
2. Section of Biological Safety Research, Chitose Laboratory, Japan Food Research Laboratories, Chitose, Japan
3. Department of Endocrinology, Metabolism and Nephrology, Kochi Medical School, Kochi University, Nankoku, Japan
4. Department of Histology, Faculty of Veterinary Medicine, Zagazig University, Zagazig, Egypt

Running head: Renal pathology in *Casp3*-KO mice

***Corresponding author: Osamu Ichii, DVM, PhD,**

Laboratory of Anatomy, Department of Basic Veterinary Sciences, Faculty of Veterinary Medicine, Hokkaido University, Kita 18, Nishi 9, Kita-ku, Sapporo 060-0818, Japan.

Email: ichi-o@vetmed.hokudai.ac.jp

Tel: +81-11-706-5189, Fax: +81-11-706-5189

Abstract

Caspase (CASP) 3 is known as a representative effector CASP of apoptosis, and recently as a mediator in inflammatory cell death called pyroptosis. Interestingly, homozygotes of *Casp3* knockout (KO) mice with 129-background shows complete embryonic lethality, however, some of those with C57BL/6 (B6)-background (B6.129S1-*Casp3*^{tm1Flv}/J) survived in lower rate (KO; 11%, WT; 22%), developing immune abnormality-associated renal phenotypes. Homozygotes of *Casp3* KO mice with B6-background that survived for 8-12 months showed abnormality in the kidney and spleen but not in the other organs. Briefly, these *Casp3* KO kidneys showed proliferative glomerular lesions characterized by increased cells, matrices, immune-complex depositions containing IgA and complement 3 in the mesangial area, podocyte injuries, and inflammatory cell infiltrations in the tubulointerstitium. However, severe membranous lesion or renal dysfunction was not observed. Increased expression of inflammation-associated gene sets and inflammatory *Casps*, including *Casp12* was observed in these *Casp3* KO kidney. Moreover, these *Casp3* KO mice showed mild splenomegaly compared with WT mice. Thus, the long-surviving *Casp3* KO mice with B6-background developed renal lesions with altered immune conditions. CASP3 deficiency and aging factors could affect this phenotype by altering the function and/or development of each cell in the kidney and immune organs.

Keywords

Kidney, Glomerulus, Caspase 3, Knockout, Immunity

Acknowledgments

The research described in this manuscript was chosen for the Encouragement Award (undergraduate section) at the 161th Japanese Association of Veterinary Anatomists in Ibaraki (11–13 September 2018, Mr. Suzuki).

Introduction

In mammals, the caspase (CASP) family is a group of cysteine proteases constituting essential components of the apoptosis signalling pathway. Humans have CASP1-10, 12, and 14, whereas mice have CASP1-4, 6-9, 12, and 14 (Degterev et al. 2003; Ho and Hawkins 2005). In a study by Ho *et al* it was reported that at the initiation of cell death signalling at receptors such as TNF receptor superfamily member 6 (FAS) and TNF superfamily, member 6 (FASL) or death receptor activate the CASP2 and CASP8-9, which are called initiator CASPs. They transduce the apoptotic signal and subsequently activate the effector CASPs such as CASP3, 6, and 7, disassembling the cellular proteins (Ho and Hawkins 2005). A series of such biological process is known as CASP cascade, which strictly regulates cell death, especially apoptosis. The cells that are not needed during the developmental period and auto-reactive immune cells in the maturation processes of the immune system are mainly eliminated by apoptosis (Bouillet et al. 2002; Fan et al. 2005). Further, defective cells damaged by ultraviolet rays or chemical substances are also removed by apoptosis (Roos and Kaina 2006). Thus, cell death pathway, particularly apoptosis, plays important roles in living bodies by removing specific cells to manage the adequate process of development and homeostasis.

CASPs are also involved in inflammatory cell death responses. Several mouse studies have revealed that pattern recognition receptors such as NLR family, pyrin domain containing 3 (NLRP3) recognizes a specific stimulatory ligand, and NLRP3 binds to CASP1 and the adaptor protein, forms a protein complex, called inflammasome (Mariathasan et al. 2004; Fernandes-Alnemri et al. 2007). Then, CASP1 cleaves and activates the proinflammatory cytokines such as interleukin 1 beta (IL-lβ) and IL-18, which trigger an inflammatory reaction notifying surrounding cells of danger (Aachoui et al. 2013; Abderrazak et al. 2015; He et al. 2015). Moreover, in humans and mice, CASP1 can cleave gasdermin D (GSDMD), which promotes

inflammatory cell death, called pyroptosis (Gy and Broz). Pyroptosis is regulated by inflammatory CASPs such as CASP1, 4, and 5 in humans, and CASP1 and 4 in mice (Aglietti and Dueber 2017). In mice, CASPs activate GSDMD by cleaving its carboxy- and amino-terminal (N-terminal). The N-terminal of GSDMD forms a plasma membrane pore and increases permeability, causing inflammatory cell death (Kayagaki et al. 2015; Shi et al. 2015; Sborgi et al. 2016). Further, in mice, pyroptosis is mainly caused by intracellular invasion of pathogenic bacteria such as *Salmonella enterica* (Fink and Cookson 2007). Cell death induces pyroptotic cells to secrete inflammatory cytokines such as IL-1β and IL-6 and cause inflammation, which is useful for defence against pathogens (Aachoui et al. 2013; Shi et al. 2017).

Therefore, CASPs are closely associated with cell death as well as immunity. Further, their abnormalities are reported to be involved in some immune-associated refractory diseases. Briefly, CASP8-deficient mice lack Paneth cells and show reduced number of goblet cells in the ileum, and inflammatory lesions are formed at the same site, suggesting a central role of CASP8 in gut mucosal immunity (Günther et al. 2011). These pathological features are similar to Crohn's disease in humans. In humans, it has been shown that the heterozygous mutation of CASP10 is responsible for autoimmune lymphoproliferative syndrome type II (Wang et al. 1999). Thus, the pathological correlations between immune-associated diseases and genetic mutations were mainly found in initiator CASPs, but scarce in effector ones because their mutants died due to embryonic lethality in mice (Zheng et al. 1999). In mice and humans, CASP3 is one of the most popular effector CASPs, which is activated by initiator CASPs such as CASP8 (Fan et al. 2005). Then, it proceeds to the final stage of apoptosis by disassembling the intracellular target proteins. Therefore, CASP3 plays extremely important roles in development and cell death through apoptosis (Bergmann and Steller 2010; Porter and Ja 2015). Importantly, CASP3 causes pyroptosis by cleaving and activating gasdermin E which is related

to GSDMD in mice and humans (Gy et al. 2017; Wang et al. 2017). Thus, CASP3 plays important roles in apoptosis as well as in inflammatory responses, and its functional deficiency would be critical for cell death and the immune system. Interestingly, CASP3-deficient mice showing a unique phenotype associated with autoimmune abnormality was also discovered.

B6.129S1-*Casp3*^{tm1Flv}/J (*Casp3* KO) mice were previously developed and used to analyse the role of CASP3 mainly in the developmental period (Kulda et al. 1996). Importantly, homozygotes of *Casp3* KO mice showed embryonic lethality with a certain probability, but upon careful investigation of the surviving homozygotes it was found that they showed unique kidney lesions and immune abnormalities. Since there is no basic and clinical evidence associated with CASP3 abnormality in the kidney and immune system organs, this study can justify the role of CASP3 as a disease-causing factor. This study raises a novel possibility for further elucidating the pathology of unknown refractory disease, especially focusing on the abnormalities between cell death and immunity.

Materials and Methods

Animal ethics

Animal experimentation was approved by the Institutional Animal Care and Use Committee of the Graduate School of Veterinary Medicine, Hokkaido University (approval No. 15-0079, 16-0124). Experimental animals were handled in accordance with the Guide for the Care and Use of Laboratory Animals, Graduate School of Veterinary Medicine, Hokkaido University (approved by the Association for Assessment and Accreditation of Laboratory Animal Care International).

Genotyping

Casp3 KO mice were purchased from the Jackson Laboratory (Bar Harbor, ME, USA). The genotyping polymerase chain reaction (PCR) amplification was performed according to the Jackson Laboratory protocol https://www2.jax.org/protocolsdb/f?p=116:5:0::NO:5:P5_MASTER_PROTOCOL_ID,P5_JRS_CODE:28532,006233, version June 14, 2017).

Sample collection, serological analysis, and urinalysis

Eight to twelve months old mice were used. Urine from each mouse was collected by applying pressure to the caudal area of the back and stored at -30 ˚C. Blood collected from femoral artery under the deep anaesthesia with the mixture of medetomidine (0.3 mg/kg), midazolam (4 mg/kg), and butorphanol (5 mg/kg) was centrifuged to obtain serum. All mice were euthanized by cervical dislocation. The spleen weight / body weight (SPW/BW) ratio was calculated. Serum concentrations of anti-double-stranded DNA (dsDNA) antibody and IgA were

134 measured by enzyme-linked immunosorbent assay (ELISA) using Lbis® Mouse Anti-dsDNA
135 ELISA KIT, AKRDD-061 (Shibayagi Co. Ltd., Gunma, Japan) and ARG81183 Mouse IgA
136 ELISA Kit (Arigo Biolaboratories Corp, Hsinchu, Taiwan) according to the manufacturer's
137 instructions, respectively. To evaluate the renal function, the serum concentrations of blood urea
138 nitrogen (BUN) and creatinine (CRE) were measured by Fuji Drichem (Fujifilm Medical Co.
139 Ltd., Tokyo, Japan). Urinary concentrations of CRE and albumin (ALB) were measured using
140 Urinary One-Step Creatinine Assay (Detroit R&D, Inc., Detroit, MI, USA) and A Murine
141 Microalbuminuria ELISA (Exocell, Philadelphia, PA, USA) according to the manufacturer's
142 instructions, respectively.
143
144 ***Tissue preparation***
145 The systemic organs including spleen, kidney, salivary glands, thymus, liver, adrenal
146 glands, testis, ovary, uterus, stomach, duodenum, jejunum, ileum, cecum, and colon were fixed
147 with 4 % paraformaldehyde (PFA) at 4 ℃ overnight. For gene expression analysis, a part of
148 kidneys was kept in RNAlater solution (Thermo Fisher Scientific, Waltham, MA, USA). For
149 the renal histopathological analysis, kidneys from some of the animals were fresh-frozen in
150 optimal cutting temperature (O.C.T.) compound (Diagnostic Biosystems, Pleasanton, CA, USA)
151 using liquid nitrogen and isopentane for immunofluorescence. Kidneys from remaining animals
152 were fixed by the combination of 2 % PFA and 2.5 % glutaraldehyde for 3-4 hours at 4 ℃ for
153 transmission electron microscopy (TEM).
154
155 ***Histopathological analysis***

Tissues fixed with PFA were processed and embedded in paraffin, cut in 3 μm thick sections, and stained in haematoxylin-eosin (HE) staining. Moreover, the kidney sections were stained by periodic acid-Schiff (PAS), Masson's trichrome (MT), periodic acid-methenamine silver (PAM), and direct fast scarlet staining (DFS) staining.

Immunostaining

Fresh-frozen kidney sections were dried for 30 minutes and washed 3 times in phosphate-buffered saline (PBS). Paraffin sections (3 μm thick) were deparaffinized followed by antigen retrieval. For immunohistochemistry, sections were soaked in methanol containing 0.3 % H_2O_2 for 20 minutes at room temperature for removal of endogenous peroxidase. After washing 3 times with PBS, sections were incubated with the blocking serum for 1 hour at room temperature and primary antibodies overnight at 4 ℃. After washing 3 times with PBS, sections were incubated with secondary antibodies for 30 minutes at room temperature and washed 3 times with PBS again. For immunofluorescence, sections were sealed with water-soluble encapsulant and observed under fluorescence microscopy (BZX-710, Keyence, Osaka, Japan). For immunohistochemistry, the sections were incubated with Streptavidin conjugated horseradish peroxidase [SABPO(R) kit; Nichirei, Tokyo, Japan] for 30 minutes and washed 3 times in PBS. For visualization of the positive reaction, the sections were incubated with 3,3′-diaminobenzidine tetrahydrochloride-H_2O_2 solution. The sections were slightly stained with haematoxylin. The details of antibody, antigen retrieval, and blocking are listed in Supplementary Table S1.

TEM

After fixation by the combination of 2 % PFA and 2.5 % glutaraldehyde for 3-4 hours at 4 ℃, samples were washed with 0.1 M phosphate buffer (PB) for 5 times, post-fixed with 1 % osmium tetroxide for 2 hours, and washed with 0.1 M PB 5 times. The samples were dehydrated with serially diluted ethanol, immersed in QY-1, and embedded into epoxy resin. Ultrathin sections (50 nm) were stained with uranium acetate and lead citrate, and observed under TEM (JEM-1210; JEOL, Tokyo, Japan).

Histoplanimetry

Fifty glomeruli were randomly selected from PAS stained kidney sections and their PAS-positive area for mesangial area, the total nuclear number, and glomerular size were measured in glomerulus by using BZ-X Analyzer (Keyence, Osaka, Japan). In 20 fields or in 20 glomeruli in tissue sections for immunohistochemical analysis, CD3- or B220-positive cells were enumerated. These parameters were compared between wild-type (WT) and KO mice. Abnormality was noted in these parameters of KO mice whereas WT mice showed normal parameters. The optimal cut-off value between normal and abnormal was analysed in each parameter by receiver operating characteristic (ROC) curve with JMP 13 (SAS Institute Japan Co., Ltd., Tokyo, Japan). Then, the ratio of normal and abnormal values was compared between WT and KO mice.

RNA extraction and analysis

Total RNA was extracted from kidney samples stored in RNAlater solution (Thermo Fisher Scientific) using the TRIzol reagent (Thermo Fisher Scientific) according to the manufacturer's instructions. The extracted total RNA was used as a template to synthesize complementary DNA

(cDNA) using ReverTra Ace® qPCR RT Master Mix (TOYOBO CO., LTD.; Osaka, Japan). Quantitative PCR (QPCR) analysis was performed on the cDNA using THUNDERBIRD® SYBR® qPCR Mix (TOYOBO CO., LTD.) and the respective gene-specific primers (See Supplementary Table S2). The QPCR analysis cycling conditions were: 95 ℃ for 1 min, 40 cycles of 95 ℃ for 15 seconds, 60 ℃ for 45 seconds. Data were normalized by the values of beta-actin (*Actb*), and those of WT by using the delta-delta Ct method.

Microarray

Four RNA samples were collected from each female WT and KO mice, and purified using the RNeasy® Micro Kit (QIAGEN, Hilden, Germany) following the manufacturer's protocol. Pooled one sample in each group was prepared, and the quality of RNA was determined by Agilent 2100 BioAnalyzer series II (Agilent, Santa Clara, CA, USA). The synthesis of cDNA and labelling of complementary RNA (cRNA) were performed by Low Input Quick Amp Labeling Kit (Agilent). Hybridization was performed by using Gene Expression Hybridization Kit and SurePrint G3 Mouse 8 x 60K ver.2.0 (Agilent). Scanning, quantification, and normalization were performed by Agilent Technologies Microarray Scanner (Agilent), Agilent Feature Extraction 12.0.3.1 (Agilent), and GeneSpring GX 14.9 (Agilent), respectively. For gene ontology (GO) analysis focusing on biological process, STRING (ELIXIR, Cambridgeshire, UK) was used.

Statistical analysis

The results expressed as the mean ± standard error (SE) and analysed in the non-parametric manner. The significance between 2 groups was analysed by Mann-Whitney's *U*-test ($P < 0.05$).

The correlation between 2 parameters was analysed using Spearman's rank correlation coefficient ($P < 0.05$). For GO analysis, false discovery rate was applied.

Results

Genotyping and protein expression of CASP3

In PCR-based genotyping (Fig. 1a), WT and KO mice showed the bands of 320 and 300 bp, respectively. Heterozygote (HT) mice showed both bands. During their breeding, the birth rate of homozygotes in *Casp3* KO mice, HT, and WT was 11% (11/101), 67% (68/101), and 22% (22/101), respectively. Next, immunohistochemistry was performed to detect CASP3 in the collected organs (Fig. 1b and c). In WT mice, nuclear CASP3-positive reactions were observed in the thymus, spleen, and intestine. However, KO mice showed no reactions in these organs. In the kidney, no CASP3-positive cell was observed in both strains (Fig. 1d).

Glomerular lesions found in KO mice

No histopathological change was observed in the systemic organs (nasopharyngeal parts, spleen, salivary glands, thymus, liver, adrenal glands, testis, ovary, uterus, stomach, duodenum, jejunum, ileum, cecum, and colon) checked (data not shown), except for the kidney of 8-12-month-old mice (Fig. 2a and b). Briefly, in the kidney of aged KO mice, the glomerular proliferative lesions including increased mesangial cells and matrixes were observed diffusely in both sexes, and the severity of them differed in glomeruli. No renal lesion was noted in WT mice. For histoplanimetry (Fig. 2c), mesangial area and nuclear number in the glomerulus was significantly increased in KO mice compared to those in WT mice in both sexes ($P < 0.01$); however, only in the male group, glomerular size was significantly increased in KO mice compared to WT mice ($P < 0.05$).

Next, percentage of dividing normal and abnormal glomeruli in each histological parameter was analysed using ROC curve at 8-12 months of age (Fig. 2d). The ratio of abnormal glomeruli in mesangial area and nuclear number was significantly higher in KO mice compared with WT

mice in both sexes ($P < 0.01$). Only in the male group, abnormally large glomeruli were seen in KO mice compared to those in WT mice ($P < 0.05$).

Characteristics of glomerular lesions in KO mice

As shown in Fig. 2B, pathological assessments were carried out for female glomeruli at 8–12 months of age because female glomeruli tended to show the higher values than male glomeruli. As shown in Fig. 3a and b, for the MT staining in females, the aniline blue-stained area in the glomerulus, indicating the sclerotic area, was slightly increased in KO mice compared to WT mice. Further, PAM and DFS staining revealed that there is no glomerular membranous lesion and amyloid deposition in the glomerulus of both strains. Immunofluorescence staining using fresh frozen sections (Fig. 3c and d) revealed that global IgA- and complement 3 (C3)-positive reactions were more strongly observed in the mesangial regions of KO mice than WT mice, whereas there was no strain difference in those of IgG- and IgM-positive reactions. Ultrastructural observation under TEM revealed that high-electron dense materials were localized to the increased mesangial area in the glomerulus of KO mice, indicating the immune complex depositions (Fig. 3e).

Glomerular cell injury and renal function in KO mice

Next, the author investigated glomerular cell injuries at 8-12 months of ages. In immunofluorescence for podocyte markers including podocin, synaptopodin, and Wilms tumour 1 homolog (WT1) in females, their positive area decreased in KO mice glomerulus compared to WT mice, particularly those of podocin and synaptopodin were localized to peripheral regions of glomerulus in KO mice (Fig. 4a and b). In TEM analysis, WT mice showed normal structure of podocytes, but podocyte foot process effacements were partially observed in KO mice (Fig.

4c). For renal functional analysis, the serum levels of BUN and CRE and urinary ALB/CRE ratio were not significantly different between WT and KO mice in both sexes (Fig. 4d).

Altered immunity in KO mice

From the IgA deposition in the glomerulus of KO mice (Fig. 3), the serum IgA level was analysed at 8-12 months of age, but statistical significance was not detected between both strains (Fig. 5a). Further, we also analysed the serum levels of anti-dsDNA antibody for autoimmune disease indices, and these tended to be higher in KO mice than in WT mice in both sex without significant differences. In the indices of systemic immune abnormalities, SPW/BW of KO mice was significantly higher than WT mice in both sexes ($P < 0.01$).

In immunohistochemistry (Fig. 5b), CD3-positive T-cells were scarcely observed in the kidney of WT females, but they were abundantly detected in KO females, especially in their tubulointerstitium at 8-12 months of age. Compared to T-cells, B220-positive B-cells were relatively scarce in the both strains. In histoplanimetry, the number of CD3- or B220-positive cell in glomerulus did not differed between female WT and KO mice, but that in tubulointerstitium significantly increased in KO mice than in WT mice ($P < 0.01$) (Fig. 5c).

Fig. 5d showed the gene expression levels of CASP family and apoptosis- or inflammation-associated molecules in the female kidney at 8-12 months of ages by QPCR analysis. For CASPs, the expression levels of inflammatory CASPs including *Casp1*, *Casp4*, and *Casp12* tended to be higher in KO mice than in WT mice, and the difference was significant for *Casp12* ($P < 0.05$). Expression of apoptosis-related molecules including DNA fragmentation factor, alpha subunit (*Dffa*), TNF receptor superfamily member 6 (*Fas*), B cell leukemia/lymphoma 2 (*Bcl2*), BCL2-associated X protein (*Bax*), and Rho-associated coiled-coil containing protein kinase 1 (*Rock1*)

299 did not change between strains, but that of *Il1b* and tumor necrosis factor (*Tnf*) tended to be
300 higher in KO mice than in WT mice. Significant difference was detected in *Tnf* ($P < 0.05$).
301 We also comprehensively compared the gene expression in the kidney of WT mice and KO
302 mice and performed the GO analysis. In the GO analysis using 2-fold upregulated genes in KO
303 mice, 859 genes were detected, and Table 1 summarized the top 5 GO showing strong
304 significance. In general, inflammation or immune-related biological process of GO including
305 immune response (111 genes), immune system process (149 genes), defence response (103
306 genes), innate immune response (65 genes), and immune effector process (57 genes), were
307 detected. No GO was detected in the GO analysis using 2-fold downregulated genes in KO mice.
308
309 ***Qualitative histopathological analysis***
310 The correlation between the parameters of glomerular lesion (Fig. 2) and immune system
311 abnormality (Fig. 5) was determined by Spearman's correlation coefficient as shown in Fig. 6.
312 In all mice, the histopathological parameters for mesangial area and nuclear number of glomeruli
313 but not glomerular size were significantly and positively correlated with the SPW/BW ratio and
314 the serum levels of anti-dsDNA antibody ($P < 0.01$). In the KO mice, the histopathological
315 parameters for mesangial area (average, ratio) and nuclear number (average) were positively
316 correlated with the serum levels of anti-dsDNA antibody ($P < 0.01$). Also, the ratio of
317 glomerular size was negatively correlated with the serum levels of anti-dsDNA antibody ($P <$
318 0.05).

Discussion

In the present study, novel phenotypes associated with kidney and spleen in the homozygotes of *Casp3* KO mice with C57BL/6 (B6)-background were found. Several previous studies reported that homozygotes of *Casp3* KO mice with B6-background showed a variety of phenotypes including neuronal apoptosis reduction and hyperplasia, hearing loss, and ovarian dysfunction (Kulda et al. 1996; Woo et al. 1998; Wang and Lenardo 2000; Matikainen et al. 2001; Takahashi et al. 2001). Mainly, the developmental disorders of central nervous system (CNS) were critical for the survival of *Casp3* KO mice with B6-background, resulting in perinatal lethality (Kulda et al. 1996). Further, although *Casp3* KO mice with 129-background showed complete embryonic lethality, but those with B6-background could survive adulthood without obvious CNS defects with a low probability (Zheng et al. 1999), indicating that genetic factors, in addition to environmental, are essential to compensate or deteriorate CASP3 deficiency. In qPCR analysis, the renal expression of effector *Casps*, such as *Casp6* and *Casp7*, did not significantly differ between WT and *Casp3* KO mice with B6-background, and these data suggested the presence of a compensatory pathway of CASP3 by the other CASP and/or CASP-independent signalling to survive through adulthood in *Casp3* KO mice with B6-background. Further, the effect of CASP3 deficiency varies depending on the mouse strain, it is necessary to analyse various *Casp3* KO mice lines carrying different genetic background to elucidate exacerbating or compensating gene factors for CASP3 deficiency and clarify the direct effect of it in kidney or immune system organs, which emphasizing the importance of CASP3 deficiency in the pathogenesis of immune-associated kidney diseases.

These *Casp3* KO mice showed the renal inflammation, mild splenomegaly, and upregulation of the inflammatory gene sets, indicating their altered immune conditions due to CASP3 deficiency. Upregulation of inflammatory *Casps* such as *Casp1, 4,* and *12*, and nuclear

343 factor κβ downstream molecules such as TNF in KO mice kidney indicates the exacerbated
344 inflammation because of CASP3 deficiency. Since CASP3 is involved in the differentiation of
345 immune progenitor cells in mice (Kuranaga and Miura 2007; Lamkanfi et al. 2007). CASP3
346 deficiency is considered to affect the immune response or development of each resident cell,
347 and the accumulation of these alterations, in addition to the effect of aging, would finally form
348 the phenotype in each organ.

349 From glomerular pathological features of these *Casp3* KO mice, the author hypothesized
350 the development of IgA nephropathy in KO mice. Representative human IgA nephropathy
351 exhibits mesangial proliferation and IgA deposition to mesangial area accompanied by
352 proteinuria and haematuria, associated with the upper respiratory inflammation that exists in the
353 mucosa-associated lymphoid tissue (MALT) such as tonsil (Xie et al. 2004). However, in KO
354 mice, renal function and serum IgA antibody level were similar to WT mice. Further, the
355 morphology of MALTs in the intestine and nasopharynx did not differ between WT and KO
356 (Supplementary Fig. S1). Podocyte injuries were suggested in KO mice, but the ALB/CRE did
357 not significantly increase, indicating that lesions in KO mice were different from nephrotic
358 syndrome based on glomerulosclerosis. Further, since KO mice showed mild splenomegaly and
359 female-dominant glomerular damage, the author also considered the possibility of autoimmune
360 glomerulonephritis like lupus nephritis. However, KO mice did not show remarkable glomerular
361 membranous lesions and the significant increase of serum anti-dsDNA antibody level as found
362 in the other model mice or human (Flores-Mendoza et al. 2018; Najafi et al. 2001). Thus, the
363 glomerular pathological feature in KO mice did not completely overlap with representative
364 known diseases, and they would develop specific pathological features due to the deficient of
365 *Casp3* gene.

The correlation scores of mesangial proliferations and SPW/BW in all examined mice indicated a strong contribution of altered immunity to develop glomerular lesions in KO mice. Also, anti-dsDNA antibody level showed a strong correlation with the parameters of mesangial lesions, indicating its increasing as the result of disease progression. C57BL/6 strain usually developed age-related glomerular lesions from over 12 months of ages, including male-dominant sclerotic feature and immunocomplex depositions of IgG and IgM but not C3 (Linder et al. 1972; Yabuki et al. 2003, 2006). Therefore, aging is also considered as an important factor for causing glomerular lesions. Furthermore, KO mice at 6 months of age did not show clear glomerular lesions (Supplementary Fig. S2). On the other hand, renal lesions and immunological abnormalities of KO mice were more severe in females than males, indicating the effects of sex hormones (González et al, 2010). Although the direct effect of CASP3 deficiency to kidney resident cells was not clear in the present study, many *in vitro* studies using cultured mesangial cells reported the crucial role of CASP3 in the process of apoptosis (Mishra et al. 2005; Shimamura et al, 2003). Therefore, the difference of sensitivity to CASP3 deficiency in each kidney composing cell might also affect the development of glomerulus-specific lesions in mice.

The association between CASP deficiency and genetic disease has been reported previously in humans. Autoimmune lymphoproliferative syndrome (ALPS) is characterized by abnormal proliferation of lymphocytes due to cell death, and patients show symptoms of autoimmune disease, characterized by hepatosplenomegaly and lymph node swelling. The causes of ALPS include genetic abnormalities in FAS, the FAS ligand, and CASP10, which are involved in the FAS-dependent cell death (Martínez-Feito et al. 2016). Furthermore, a CASP8 deficiency results in similar symptoms (Rieux-Laucat et al. 2018). Although no study has assessed the CASP3 deficiency in humans, our data potentially contribute to understanding the pathogenesis of CASP deficiency-related diseases to develop a novel therapeutic strategy.

In conclusion, the author found that survived and aged *Casp3* KO mice with B6-background exhibits the proliferative glomerular lesions characterized by the mesangial cell-associated lesions with mild sclerosis and the deposition of immune complexes including IgA and C3, and immune abnormality such as renal inflammation and altered spleen phenotypes. Since these phenotypes are specific compared with the other representative models or the patients in humans for immune-mediated renal diseases, the crucial pathological role of CASP3 in the kidney composing cells was also suggested. The author concluded that CASP3 deficiency, in addition to the aging, would develop the characteristic glomerular lesions, and these findings emphasize the importance of CASP3 deficiency as a potential causative factor of immune-associated kidney diseases.

Compliance with Ethical Statements

Conflict of Interest

The authors have no conflicts of interest directly relevant to the content of this article.

Funding

This work was supported by the research grant from KAC Co., Ltd (Dr. Ichii).

Ethical approval

Animal experimentation was approved by the Institutional Animal Care and Use Committee of the Graduate School of Veterinary Medicine, Hokkaido University (approval No. 15-0079, 16-0124). Experimental animals were handled in accordance with the Guide for the Care and Use of Laboratory Animals, Graduate School of Veterinary Medicine, Hokkaido University (approved by the Association for Assessment and Accreditation of Laboratory Animal Care International).

References

Aachoui Y, Sagulenko V, Miao EA, Stacey KJ (2013) Inflammasome-mediated pyroptotic and apoptotic cell death, and defense against infection. Curr Opin Microbiol 16:319–326. doi: 10.1016/j.mib.2013.04.004

Abderrazak A, Syrovets T, Couchie D, et al (2015) NLRP3 inflammasome: From a danger signal sensor to a regulatory node of oxidative stress and inflammatory diseases. Redox Biol 4:296–307. doi: 10.1016/j.redox.2015.01.008

Aglietti RA, Dueber EC (2017) Recent Insights into the Molecular Mechanisms Underlying Pyroptosis and Gasdermin Family Functions. Trends Immunol 38:261–271. doi: 10.1016/j.it.2017.01.003

Bergmann A, Steller H (2010) Apoptosis , Stem Cells , and Tissue Regeneration. 3:1–9

Bouillet P, Purton JF, Godfrey DI, et al (2002) BH3-only Bcl-2 family member Bim is required for apoptosis of autoreactive thymocytes. Nature 415:922–926. doi: 10.1038/415922a

Degterev A, Boyce M, Yuan J (2003) A decade of caspases. Oncogene 22:8543–8567. doi: 10.1038/sj.onc.1207107

Fan TJ, Han LH, Cong RS, Liang J (2005) Caspase family proteases and apoptosis. Acta Biochim Biophys Sin (Shanghai) 37:719–727. doi: 10.1111/j.1745-7270.2005.00108.x

Fernandes-Alnemri T, Wu J, Yu JW, et al (2007) The pyroptosome: A supramolecular assembly of ASC dimers mediating inflammatory cell death via caspase-1 activation. Cell Death Differ 14:1590–1604. doi: 10.1038/sj.cdd.4402194

Fink SL, Cookson BT (2007) Pyroptosis and host cell death responses during Salmonella infection. Cell Microbiol 9:2562–2570. doi: 10.1111/j.1462-5822.2007.01036.x

Günther C, Martini E, Wittkopf N, et al (2011) Caspase-8 regulates TNF-α-induced epithelial necroptosis and terminal ileitis. Nature 477:335–339. doi: 10.1038/nature10400

Gy ILO, Broz P Caspase target drives pyroptosis. 5–6

Gy ILO, Broz P, Khalil H, et al (2017) Cleavage of DFNA5 by caspase-3 during apoptosis mediates progression to secondary necrotic/pyroptotic cell death. Nature 547:99–103. doi: 10.1038/nature22393

He W, Wan H, Hu L, et al (2015) Gasdermin D is an executor of pyroptosis and required for interleukin-1β secretion. Cell Res 25:1285–1298. doi: 10.1038/cr.2015.139

Ho PK, Hawkins CJ (2005) Mammalian initiator apoptotic caspases. FEBS J 272:5436–5453. doi: 10.1111/j.1742-4658.2005.04966.x

Kayagaki N, Stowe IB, Lee BL, et al (2015) Caspase-11 cleaves gasdermin D for non-canonical inflammasome signalling. doi: 10.1038/nature15541

Kulda K, Zheng TS, Na S, et al (1996) Decreased apoptosis in the brain and premature lethality in CPP32- deficient mice. Nature 384:368–372. doi: 10.1038/384368a0

Mariathasan S, Hewton K, Monack DM, et al (2004) Differential activation of the inflammasome by caspase-1 adaptors ASC and Ipaf. Nature 430:213–218. doi: 10.1038/nature02664

Martínez-Feito A, Melero J, Mora-Díaz S, et al (2016) Autoimmune lymphoproliferative syndrome due to somatic FAS mutation (ALPS-sFAS) combined with a germline caspase-10 (CASP10) variation. Immunobiology 221:40–47. doi: 10.1016/J.IMBIO.2015.08.004

Matikainen T, Perez GI, Zheng TS, et al (2001) Caspase-3 gene knockout defines cell lineage specificity for programmed cell death signaling in the ovary. Endocrinology 142:2468–2480. doi: 10.1210/endo.142.6.8078

463 Porter AG, Ja RU (2015) Emerging roles of Caspase-3 in apoptosis Emerging roles of caspase-
464 3 in apoptosis. Cell Death Differ 99–104. doi: 10.1038/sj.cdd.4400476
465 Rieux-Laucat F, Magérus-Chatinet A, Neven B (2018) The Autoimmune Lymphoproliferative
466 Syndrome with Defective FAS or FAS-Ligand Functions. J Clin Immunol 38:558–568.
467 doi: 10.1007/s10875-018-0523-x
468 Roos WP, Kaina B (2006) DNA damage-induced cell death by apoptosis. Trends Mol Med
469 12:440–450. doi: 10.1016/j.molmed.2006.07.007
470 Sborgi L, Rühl S, Mulvihill E, et al (2016) GSDMD membrane pore formation constitutes the
471 mechanism of pyroptotic cell death. 35:1766–1778
472 Shi J, Gao W, Shao F (2017) Pyroptosis: Gasdermin-Mediated Programmed Necrotic Cell
473 Death. Trends Biochem Sci 42:245–254. doi: 10.1016/j.tibs.2016.10.004
474 Shi J, Zhao Y, Wang K, et al (2015) Cleavage of GSDMD by inflammatory caspases
475 determines pyroptotic cell death. doi: 10.1038/nature15514
476 Takahashi K, Kamiya K, Urase K, et al (2001) Caspase-3-deficiency induces hyperplasia of
477 supporting cells and degeneration of sensory cells resulting in the hearing loss. Brain Res
478 894:359–367. doi: 10.1016/S0006-8993(01)02123-0
479 Wang J, Lenardo MJ (2000) Roles of caspases in apoptosis, development, and cytokine
480 maturation revealed by homozygous gene deficiencies. J Cell Sci 113 (Pt 5:753–757
481 Wang J, Zheng L, Lobito A, et al (1999) Inherited human caspase 10 mutations underlie
482 defective lymphocyte and dendritic cell apoptosis in autoimmune lymphoproliferative
483 syndrome type II. Cell 98:47–58. doi: 10.1016/S0092-8674(00)80605-4
484 Wang Y, Gao W, Shi X, et al (2017) Chemotherapy drugs induce pyroptosis through caspase-
485 3 cleavage of a gasdermin. Nature 547:99–103. doi: 10.1038/nature22393

Woo M, Hakem R, Soengas MS, et al (1998) Essential contribution of caspase 3/CPP32 to apoptosis and its associated nuclear changes. Genes Dev 12:806–19. doi: 10.1101/gad.12.6.806

Zheng TS, Hunot S, Kuida K, Flavell RA (1999) Caspase knockouts: Matters of life and death. Cell Death Differ 6:1043–1053. doi: 10.1038/sj.cdd.4400593

Author contributions

T.S. and O.I. designed, performed experiments, and analysed data. T.N. analysed data. T.H., Y.H.A.E. and Y.K. designed and reviewed the experiments. All authors were involved in writing the manuscript and provided final approval to publish the manuscript.

498 **Table 1. Gene ontology analysis in the kidney of *Casp3* KO mice.**

	Pathway ID	Pathway description	Count in gene set	False discovery rate
Upregulated genes	**GO:0006955**	**Immune response**	**111**	**4.86E-54**
	Aif1, Aim2, Apbb1ip, Batf, Bst2, Btk, C1qa, C1qb, C1qc, C1ra, C3, C4b, Card9, Ccl12, Ccl2, Ccl3, Ccl4, Ccl5, Ccl6, Ccl7, Ccl8, Ccl9, Ccr5, Ccr6, Ccr7, Cd180, Cd300a, Cd8a, Cfd, Cfp, Clec4d, Clec4e, Clec4n, Coro1a, Ctsc, Ctss, Cxcl10, Cxcl13, Cxcl9, Cybb, Ddx58, Dhx58, Dock2, Exo1, Fasl, Fcer1g, Fcgr1, Ffar2, Fgr, Fut7, Fyb, Gch1, Gzmb, H2-D1, H2-Q10, Hck, Ifih1, Ifit1, Ifit2, Ifit3, Iigp1, Il1rn, Il5ra, Irf1, Irf7, Irg1, Irgm1, Isg15, Kit, Lck, Lcp2, Lilrb3, Lst1, Ltf, Ly86, Mefv, Mmp7, Ms4a2, Mx2, Myo1f, Myo1g, Naip6, Oas1a, Oas2, Oasl1, Oasl2, Pglyrp1, Pigr, Pik3cd, Pik3cg, Pou2f2, Rnf19b, S100a8, S100a9, Sh2d1a, Slc11a1, Star, Stat1, Stat2, Syk, Tlr1, Tlr7, Tlr8, Tnf, Tnfrsf1b, Trem2, Trim14, Tyrobp, Vav1, Vtn, Zbp1
	GO:0002376	**Immune system process**	**149**	**6.43E-51**
	AF251705, Adam8, Aif1, Aim2, Apbb1ip, Batf, Btk, Btla, C1qa, C1qb, C1qc, C1ra, C4b, C5ar1, Card11, Card9, Ccl12, Ccl2, Ccl3, Ccl4, Ccl5, Ccl6, Ccl7, Ccl8, Ccl9, Ccr5, Ccr6, Ccr7, Cd180, Cd300a, Cd300e, Cd300ld, Cd300lh, Cd3d, Cd8a, Cfd, Cfp, Chia, Clec4d, Clec4e, Clec4n, Coro1a, Ctsc, Ctss, Cxcl10, Cxcl13, Cxcl9, Cxcr3, Cybb, Ddx58, Dhx58, Dock2, Dock7, Emr1, Ercc2, Exo1, Fasl, Fcer1g, Fcgr1, Ffar2, Fgr, Fut7, Fyb, Gch1, Gfi1, Gzmb, H2-Q10, Hck, Hp, Ifih1, Ifit1, Ifit2, Ifit3, Iigp1, Ikzf1, Ikzf3, Il1rn, Il33, Il5ra, Il7r, Irf1, Irf7, Irg1, Irgm1, Isg15, Itga4, Itgax, Itgb2, Kit, Lck, Lcp2, Lilrb3, Lilrb4, Lst1, Ltf, Ly86, Mefv, Mfap5, Mmp7, Ms4a2, Mx2, Myo1f, Myo1g, Naip6, Nfam1, Oas1a, Oas2, Oasl1, Oasl2, Pdcd1, Pglyrp1, Pigr, Pik3ap1, Pik3cd, Pik3cg, Pilrb1, Pla2g2d, Plek, Pou2f2, Ptpn22, Ptprc, Rab33a, Rnf19b, Runx2, S100a8, S100a9, Selplg, Serpina3g, Sh2d1a, Slc11a1, Spib, Spn, Star, Stat1, Stat2, Syk, Tap1, Themis2, Tnf, Tnfrsf1b, Top2a, Trem2, Treml2, Trim14, Tyrobp, Vav1, Vcam1, Vtn, Zbp1
	GO:0006952	**Defense response**	**103**	**7.20E-39**
	A*dam8, Agtr2, Ahsg, Aif1, Aim2, Batf, Btk, C1qa, C1qb, C1qc, C1ra, C3, C4b, Card9, Ccl12, Ccl2, Ccl3, Ccl4, Ccl7, Ccl8, Ccr7, Cd180, Cd300a, Cd8a, Cfd, Cfp, Chi3l3, Chia, Clec4d, Clec4e, Clec4n, Coro1a, Cxcl10, Cxcl13, Cxcl9, Cxcr3, Cybb, Ddx58, Dhx58, Fcer1g, Fcgr1, Ffar2, Fgr, Gch1, H2-D1, Hck, Hp, Ifih1, Ifit1, Ifit2, Ifit3, Iigp1, Il33, Il5ra, Irf1, Irf7, Irg1, Irgm1, Isg15, Itgax, Kit, Lck, Ltf, Ly86, Lyz1, Lyz2, Mefv, Mmp7, Ms4a2, Mx2, Myo1f, Naip6, Nfkbid, Oas1a, Oas2, Oasl1, Oasl2, Orm1, Orm2, Pglyrp1, Pik3cd, Pik3cg, Plac8, Ptprc, Rnf19b, Saa3, Sh2d1a, Slc11a1, Spn, Star, Stat1, Stat2, Syk, Tap1, Themis2, Tlr1, Tlr7, Tlr8, Tnf, Tnfrsf1b, Trem2, Trim14, Zbp1*
	GO:0045087	**Innate immune response**	**65**	**9.99E-33**
	Aif1, Aim2, Bst2, Btk, C1qa, C1qb, C1qc, C1ra, C3, C4b, Card9, Ccl2, Ccl5, Cd180, Cfd, Cfp, Clec4d, Clec4e, Clec4n, Coro1a, Cybb, Ddx58, Dhx58, Fcer1g, Fcgr1, Fgr, Gch1, Hck, Ifih1, Ifit1, Ifit2, Ifit3, Iigp1, Irf1, Irf7, Irg1, Irgm1, Isg15, Lck, Ltf, Ly86, Mefv, Mx2, Naip6, Oas1a, Oas2, Oasl1, Oasl2, Pglyrp1, Pik3cd, Pik3cg, Rnf19b, S100a8, S100a9, Slc11a1, Star, Stat1, Stat2, Syk, Tlr1, Tlr7, Tlr8, Trem2, Trim14, Zbp1
	GO:0002252	**Immune effector process**	**57**	**3.33E-29**
	Apbb1ip, Batf, Bst2, C1qa, C1qb, C1qc, C1ra, C3, C4b, Card9, Ccl3, Cd180, Cd300a, Cd8a, Cfd, Cfp, Clec4d, Clec4e, Coro1a, Ctsc, Cxcl10, Cxcl9, Ddx58, Dhx58, Dock2, Exo1, Fcer1g, Fcgr1, Fut7, Gzmb, Ifih1, Ifit1, Ifit2, Ifit3, Il33, Irf1, Irf7, Isg15, Itgax, Kit, Lilrb3, Mx2, Myo1f, Myo1g, Oas1a, Oas2, Oasl1, Oasl2, Pou2f2, Ptprc, Rnf19b, Slc11a1, Syk, Tlr7, Tlr8, Tyrobp, Zbp1
Downregulated genes	NA			

62, 976 genes were examined. 859 genes were upregulated, and 441 genes were downregulated in the kidneys of KO mice compared with that in the kidneys of WT mice.

Figure legends

Figure 1. Genotyping and caspase 3 protein expression in mouse organs.

(a) Genotyping by polymerase chain reaction. Wild type (WT) mice showed a band of 320 bp whereas caspase 3 (*Casp3*) knockout (KO) mice showed a band of 300 bp. Heterozygotes (HT) mice showed bands of both 300 and 320 bp.

(b and c) CASP3 localization in the organs of WT and KO mice. Immunohistochemistry using females at 8 months. In WT mice, positive reactions were observed in thymus (panel b), spleen (panel b'), and epithelium or lamina propria of ileum (panel b''). There was no positive reaction in KO mice (panels c-c''). Arrowheads show positive cell. Bars = 50 μm.

(d) CASP3 localization by immunohistochemistry in kidneys of 8-month-old mice. There was no positive reaction in renal glomerulus of WT and KO mice (panels d and d'). Bars = 50 μm.

Figure 2. Glomerular pathology of caspase 3 knockout mice.

(a and b) Glomerular features in wild type (WT) mice and caspase 3 knockout (KO) mice showing normal and abnormal morphology. Periodic acid-Schiff staining using mice at 8 months. Compared with WT mice (panels a and b) and normal glomeruli of KO mice (panels a' and b'), abnormal glomeruli of KO mice showed increased nuclear number and mesangial area (panels a'' and b''). Bars = 50 μm.

(c) Histoplanimetry for mesangial area (panel c), nuclear number (panel c'), and glomerular size (panel c'') using mice at 8-12 months. Values = mean ± standard errors (SE). $^{**}P < 0.01$, $^{*}P < 0.05$, Mann-Whitney *U*-test

(d) Ratio of normal and abnormal glomeruli for mesangial area (panel d), nuclear number (panel d'), and glomerular size (panel d'') using mice at 8-12 months. Threshold was

525 determined by receiver operating characteristic analysis of each glomerulus parameter.
526 Values = mean ± SE. $^{**}P < 0.01$, $^{*}P < 0.05$, Mann-Whitney *U*-test.
527
528 **Figure 3. Characteristics of glomerular pathology in caspase 3 knockout mice.**
529 **(a and b)** Glomerular pathology of females at 8 months. Mild sclerosis was observed in caspase
530 3 knockout (KO) mice (panel b), but not in wild type (WT) mice (panel a) in Masson's
531 trichrome (MT) staining. No membranous lesion or amyloid deposit was observed in both
532 WT (panels a' and a'') and KO mice (panels b' and b'') in periodic acid-methenamine silver
533 (PAM) and direct fast scarlet staining (DFS). Square in PAM staining shows the normal
534 glomerular basement membrane in KO mice. Bars = 50 μm.
535 **(c and d)** Immunofluorescence for immune-complex detection using fresh frozen sections from
536 females at 8 months. IgA- (panel d) and complement 3 (C3, panel d'')-positive reactions
537 are observed in the mesangial area of KO mice, but not in WT mice (panels c and c'').
538 Positive reactions for IgG and IgM are not observed in both mice (panels c', c''', d', and
539 d'''). Bars = 50 μm.
540 **(e)** Transmission electron microscopy (TEM) using females at 8 months. Increased mesangial
541 cells and its area are observed in KO mice (panel e). Square area indicates that high-electron
542 dense materials (showed by arrows) are observed in the mesangial area of KO mice (panel
543 e'). Cap: capillary. Mes: mesangial cells. Bars = 2.0 μm.
544
545 **Figure 4. Glomerular cell injury and renal function of caspase 3 knockout mice.**
546 **(a and b)** Peripherally altered reactions of podocin, synaptopodin, and Wilms tumor 1 homolog
547 (WT-1) expression are observed in caspase 3 knockout (KO) mice (panels b-b''), but not

548 in wild type (WT) mice (panels a-a''). Immunofluorescence using females at 8 months.
549 Bars = 50 μm.
550 **(c)** Transmission electron microscopy (TEM) using females at 8 months. Foot process
551 effacements (showed by arrows) of podocytes are observed in KO mice (panel c'), but not
552 in WT mice (panel c). Cap: capillary. Lu: lumens of Bowman's capsule. Bars = 2.0 μm.
553 **(d)** Measurement of the serum blood urea nitrogen (BUN, panel d), serum creatinine (CRE,
554 panel d'), the ratio of urinary albumin (ALB) to CRE (panel d'') using mice at 8-12 months.
555 Values = mean ± standard errors (SE). Mann-Whitney *U*-test.
556
557 **Figure 5. Altered systemic and renal immunity in caspase 3 knockout mice.**
558 **(a)** Measurement of serum IgA antibody (panel a) and anti-double-stranded DNA (dsDNA)
559 antibody levels (panel a') and the ratio of spleen weight (SPW)/body weight (BW, panel
560 a'') in wild type (WT) and caspase 3 knockout (KO) mice using mice at 8-12 months.
561 Values = mean ± standard errors (SE). $^{**}P < 0.01$, Mann-Whitney *U*-test.
562 **(b)** Localizations of CD3- or B220-positive cells in the kidney. Immunohistochemistry using
563 females at 8 months. Each positive cell is observed in caspase 3 knockout (KO) mice
564 (panels b' and b'''), but few in wild type (WT) mice (panels b and b''). Bars = 100 μm.
565 **(c)** Measurement of the number of CD3- or B220-positive cells in glomerulus (Glo, panels c
566 and c') and tubulointerstitium (Ti, panels c'' and c''') using females at 8-12 months. Values
567 = mean ± standard errors (SE). $^{**}P < 0.01$, Mann-Whitney *U*-test.
568 **(d)** Gene expression analysis for caspase family (panel d), apoptosis, and inflammation (panel
569 d') in the kidneys of females at 8-12 months. Quantitative PCR analysis. Values = mean ±
570 standard errors (SE). $^{*}P < 0.05$, Mann-Whitney *U*-test.
571

Figure 6. Correlation between glomerular histopathology and systemic immune alternation in caspase 3 knockout mice.

(a-c) Correlations between the parameters of glomerular histopathology for mesangial area (panels a and a'), nuclear number (panels b and b'), and glomerular size (panels c and c') and spleen weight (SPW)/body weight (BW).

(d-f) Correlations between the parameters of glomerular histopathology for mesangial area (panels d and d'), nuclear number (panels e and e'), and glomerular size (panels f and f') and serum level of anti-double stranded DNA (dsDNA) antibody level.

*P < 0.05, **P < 0.01. Spearman's rank correlation coefficient. Black points: wild type (WT) mice. Red points: caspase 3 knockout (KO) mice. For statistical analysis, "All" included both sexes of WT (n = 8) and KO mice (n = 12), and "KO" included KO mice only. Black and red dotted lines indicated the approximate curves in "All" and "KO", respectively.

Figure 1

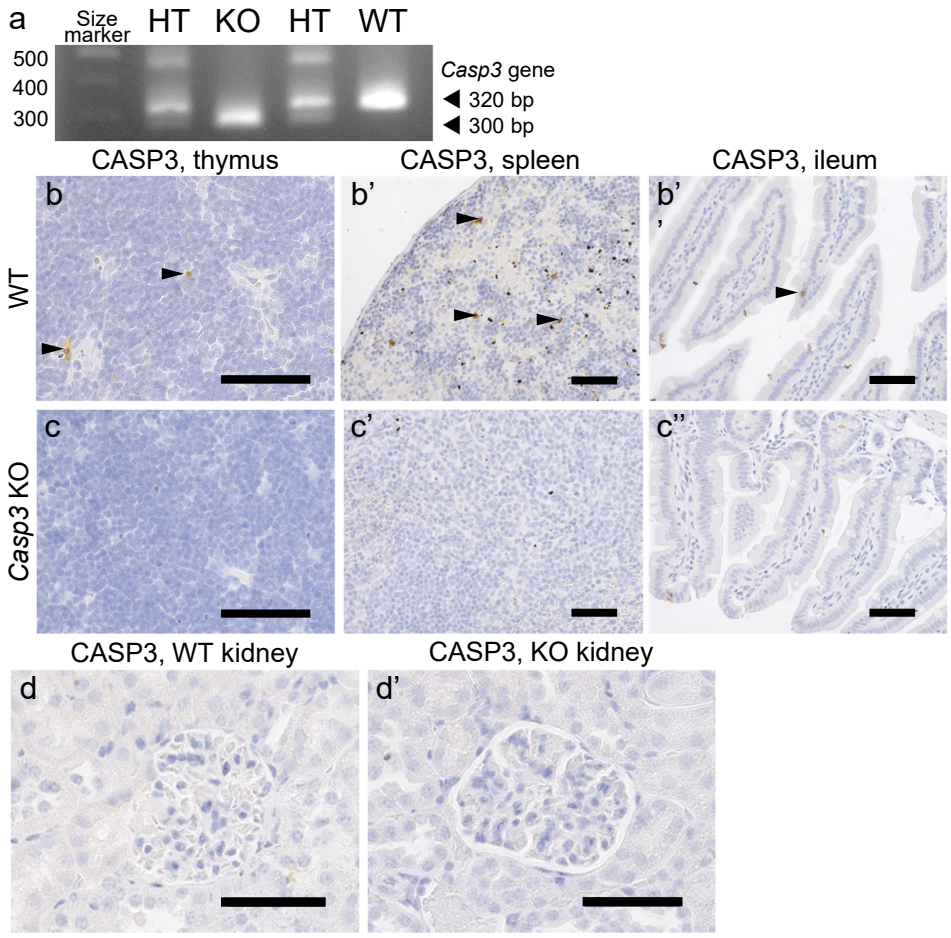
a
Size marker
HT
KO
HT
WT
500
400
300
Casp3 gene
320 bp
300 bp
CASP3, thymus
CASP3, spleen
CASP3, ileum
b
b'
b''
WT
c
c'
c''
Casp3 KO
CASP3, WT kidney
CASP3, KO kidney
d
d'

Figure 2

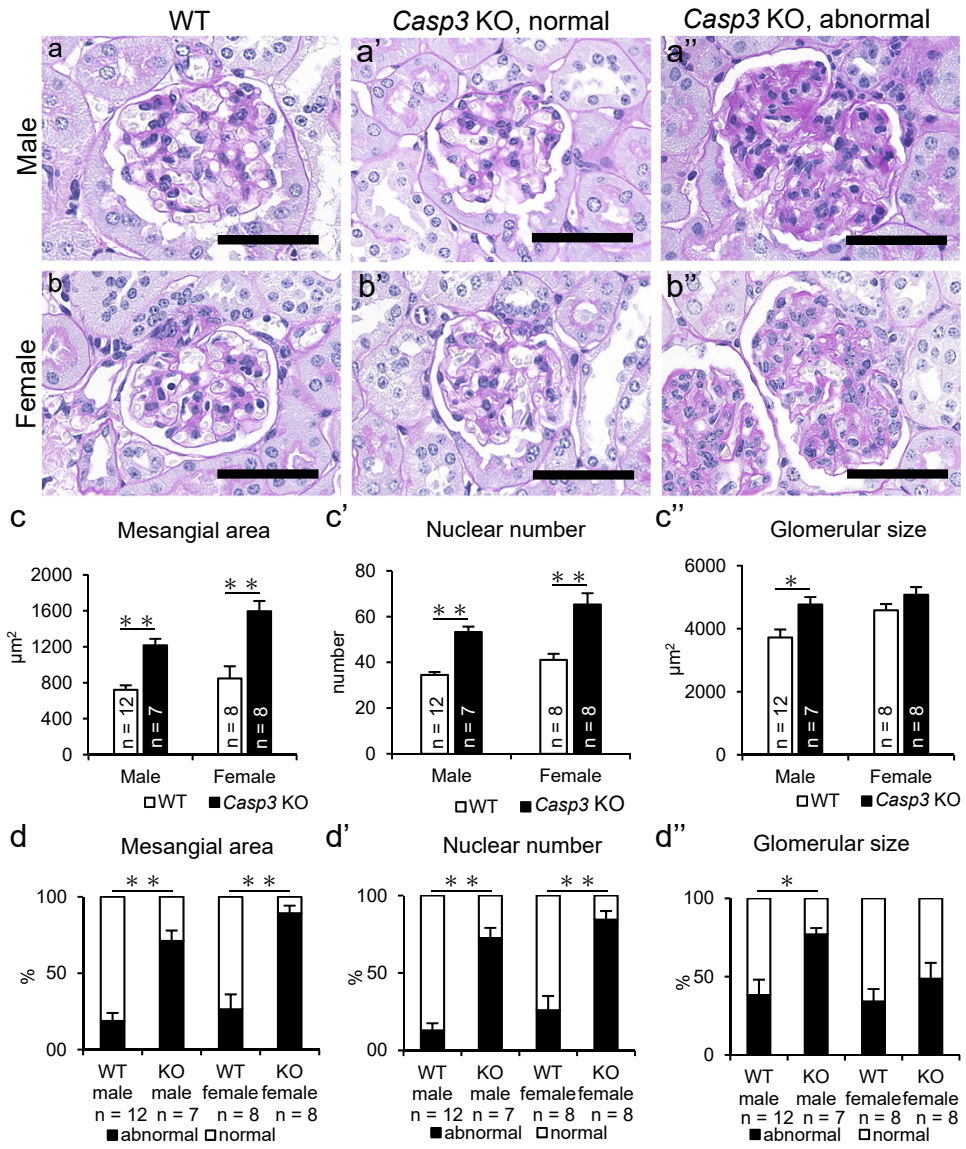
WT
Casp3 KO, normal
Casp3 KO, abnormal
a
a'
a''
b
b'
b''
Male
Female
c
Mesangial area
c'
Nuclear number
c''
Glomerular size
μm²
number
n = 12
n = 7
n = 8
n = 8
Male
Female
WT
Casp3 KO
d
Mesangial area
d'
Nuclear number
d''
Glomerular size
%
WT male n = 12
KO male n = 7
WT female n = 8
KO female n = 8
abnormal
normal

Figure 3

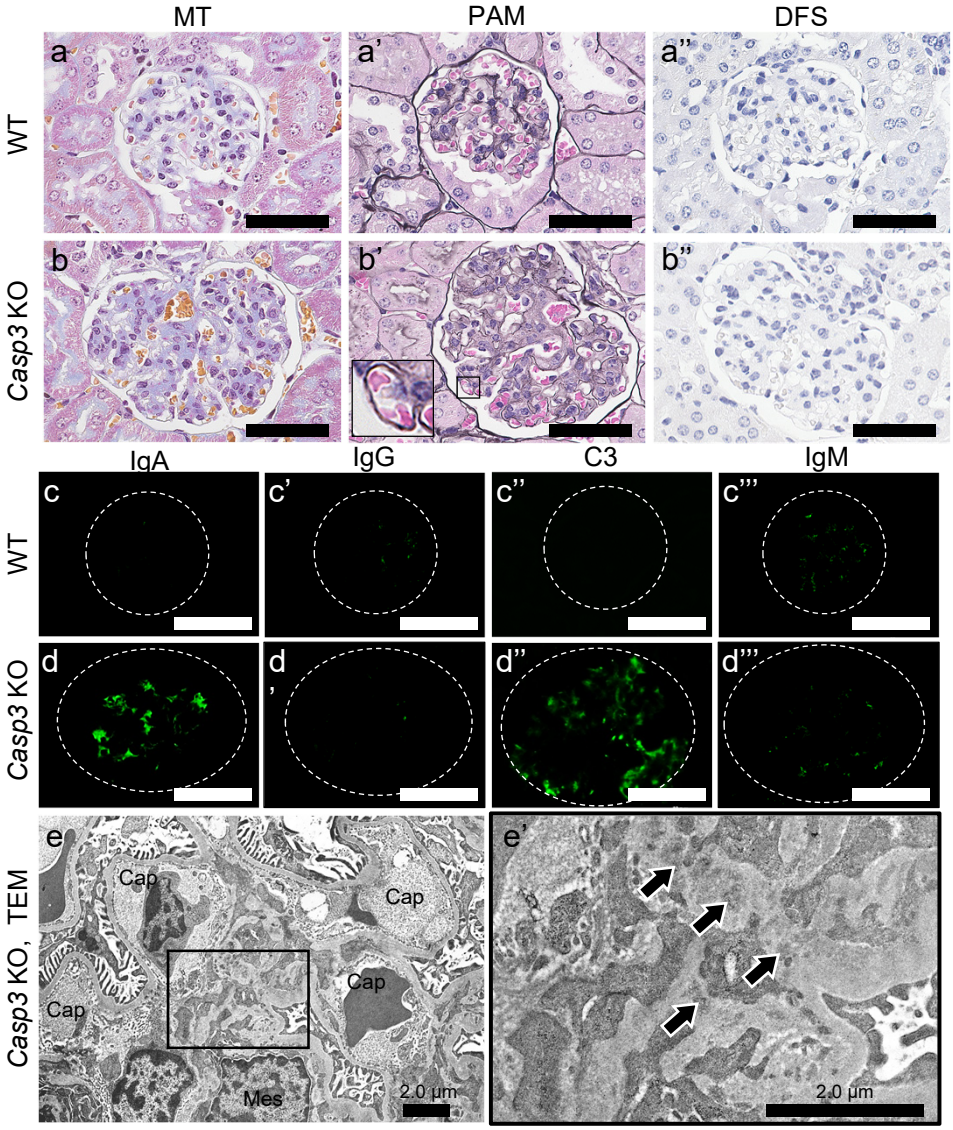
MT
PAM
DFS
WT
Casp3 KO
a
a'
a''
b
b'
b''
IgA
IgG
C3
IgM
c
c'
c''
c'''
d
d'
d''
d'''
Casp3 KO, TEM
e
e'
Cap
Cap
Cap
Cap
Mes
2.0 μm
2.0 μm

Figure 4

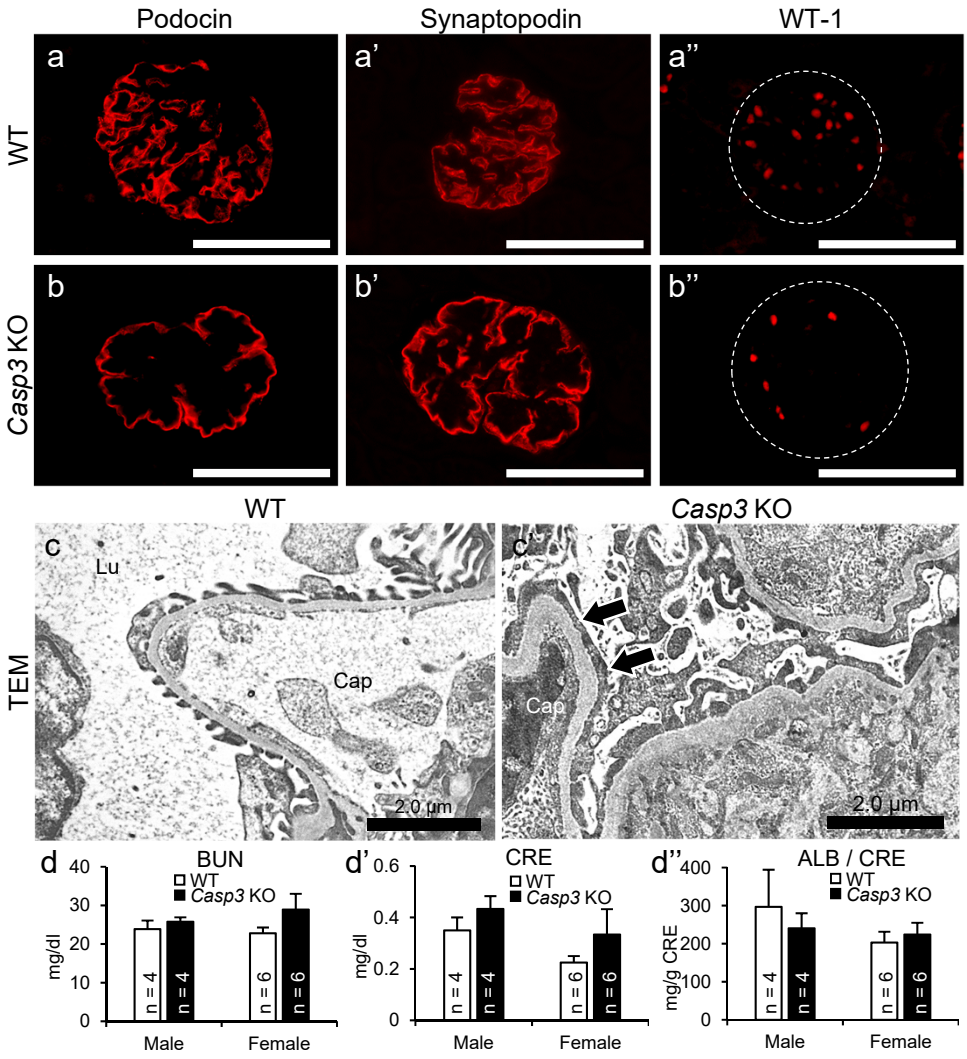
Podocin
Synaptopodin
WT-1
WT
Casp3 KO
a
a'
a''
b
b'
b''
TEM
WT
Casp3 KO
c
Lu
Cap
2.0 μm
c'
Cap
2.0 μm
d
BUN
WT
Casp3 KO
mg/dl
n = 4
n = 4
n = 6
n = 6
Male
Female
d'
CRE
mg/dl
d''
ALB / CRE
mg/g CRE

Figure 5

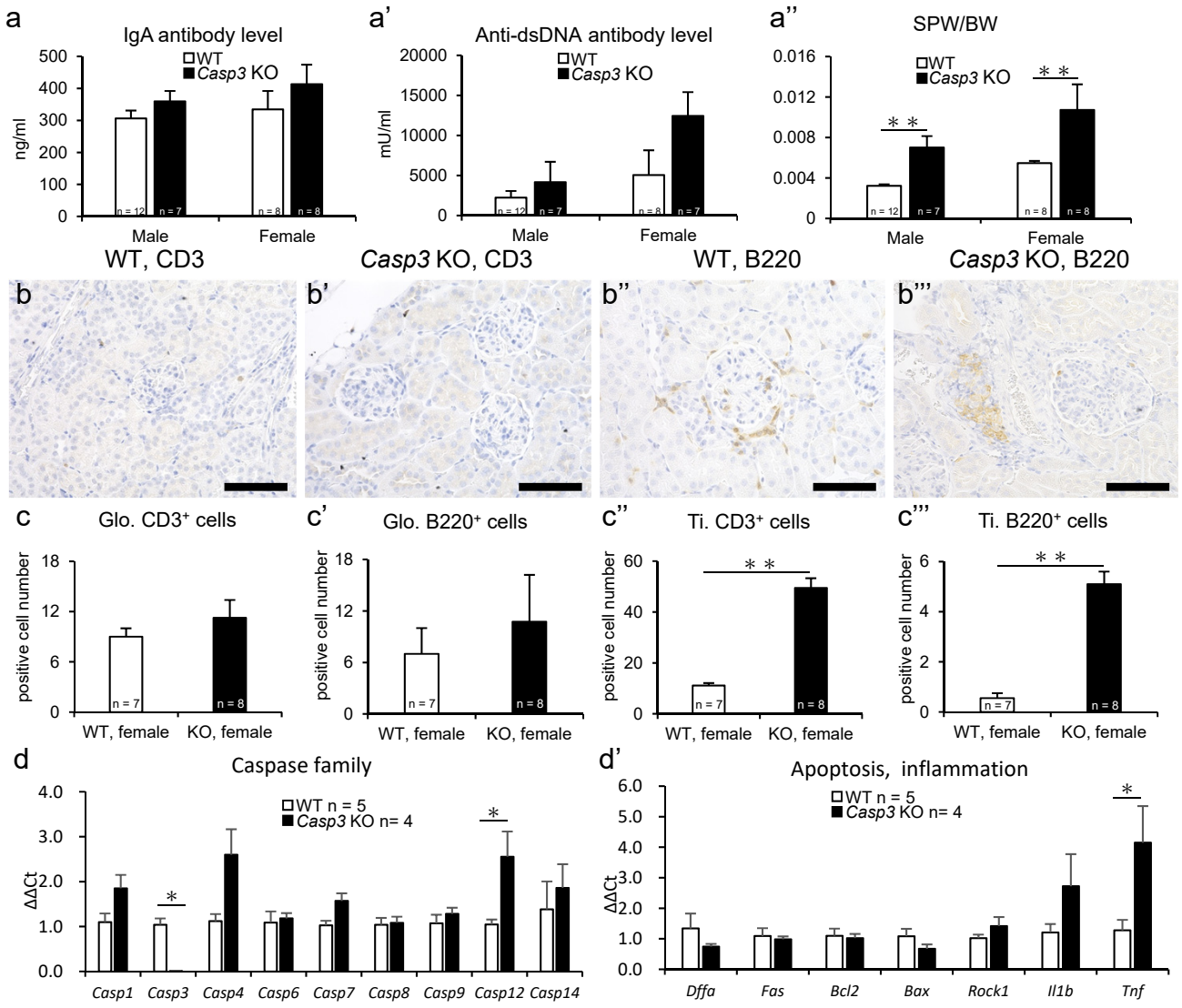
a
IgA antibody level
WT
Casp3 KO
ng/ml
Male
Female
a'
Anti-dsDNA antibody level
mU/ml
a''
SPW/BW
WT, CD3
Casp3 KO, CD3
WT, B220
Casp3 KO, B220
b
b'
b''
b'''
c
Glo. CD3+ cells
c'
Glo. B220+ cells
c''
Ti. CD3+ cells
c'''
Ti. B220+ cells
positive cell number
WT, female
KO, female
d
Caspase family
WT n = 5
Casp3 KO n= 4
ΔΔCt
Casp1
Casp3
Casp4
Casp6
Casp7
Casp8
Casp9
Casp12
Casp14
d'
Apoptosis, inflammation
Dffa
Fas
Bcl2
Bax
Rock1
Il1b
Tnf

Figure 6

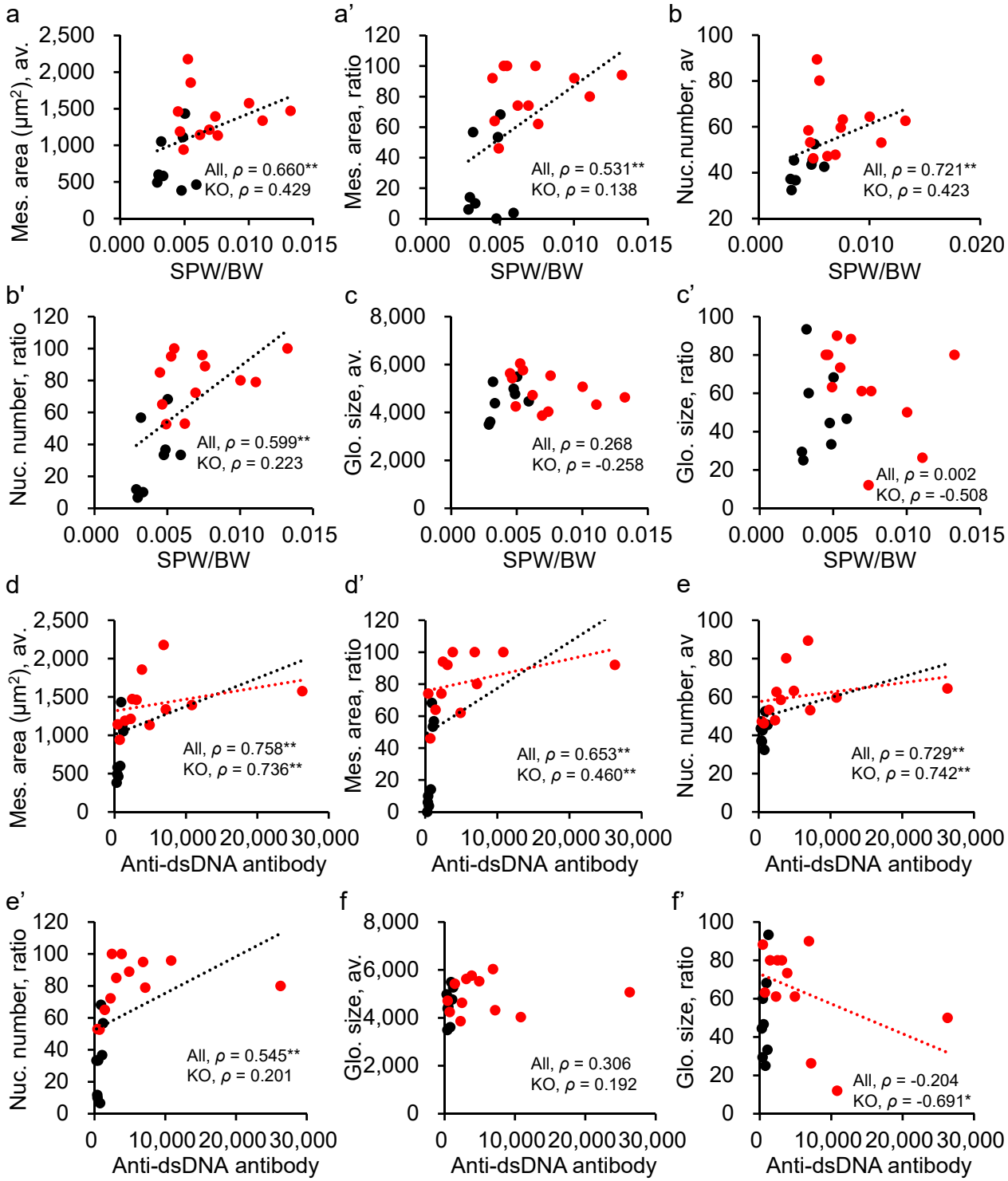
a
Mes. area (μm²), av.
SPW/BW
All, ρ = 0.660**
KO, ρ = 0.429
a'
Mes. area, ratio
SPW/BW
All, ρ = 0.531**
KO, ρ = 0.138
b
Nuc.number, av
SPW/BW
All, ρ = 0.721**
KO, ρ = 0.423
b'
Nuc. number, ratio
SPW/BW
All, ρ = 0.599**
KO, ρ = 0.223
c
Glo. size, av.
SPW/BW
All, ρ = 0.268
KO, ρ = -0.258
c'
Glo. size, ratio
SPW/BW
All, ρ = 0.002
KO, ρ = -0.508
d
Mes. area (μm²), av.
Anti-dsDNA antibody
All, ρ = 0.758**
KO, ρ = 0.736**
d'
Mes. area, ratio
Anti-dsDNA antibody
All, ρ = 0.653**
KO, ρ = 0.460**
e
Nuc. number, av
Anti-dsDNA antibody
All, ρ = 0.729**
KO, ρ = 0.742**
e'
Nuc. number, ratio
Anti-dsDNA antibody
All, ρ = 0.545**
KO, ρ = 0.201
f
Glo. size, av.
Anti-dsDNA antibody
All, ρ = 0.306
KO, ρ = 0.192
f'
Glo. size, ratio
Anti-dsDNA antibody
All, ρ = -0.204
KO, ρ = -0.691*

Supplemental figure 1

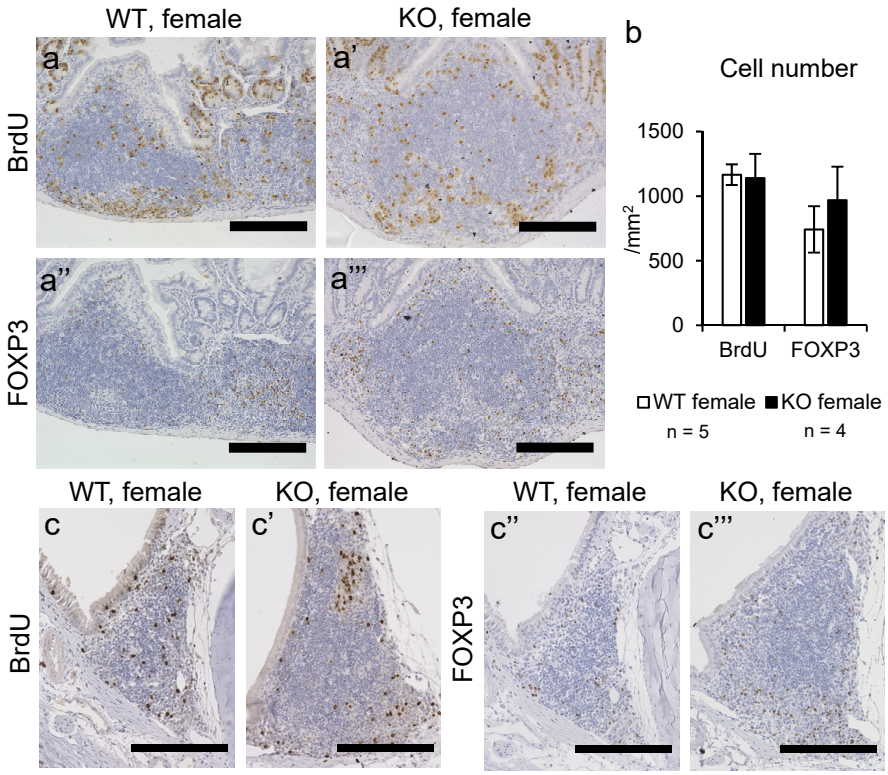

Supplemental figure 1

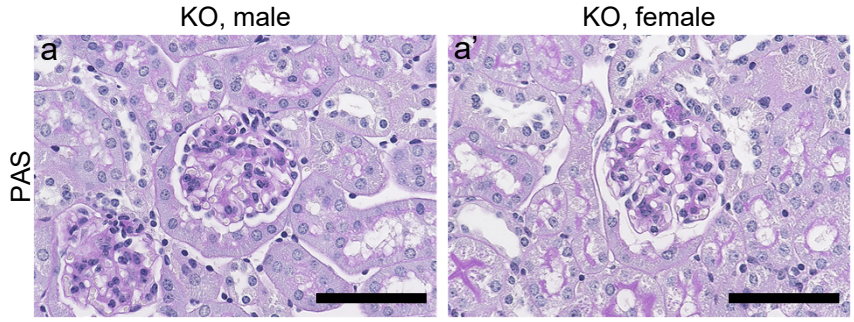

Supplementary Table S1. Antibodies used in this study.

Antibody	Host	Dilution	Source	Retrieval	Blocking	Note
CASP3	Rabbit	1:300	Cell Signaling Technology, Danvers, MA, USA	CB	10 % Goat normal serum	
CD3	Rabbit	1:200	Nichirei, Tokyo, Japan	Tris	10 % Goat normal serum	
B220	Rat	1:1600	Cedarlane, Burlington, Canada	CB	10 % Goat normal serum	
BrdU	Rat	1:400	Abcam, Cambridge, UK	CB	10 % Goat normal serum	Supplemental figure S1
FOXP3	Rat	1:400	Thermo Fisher Scientific, Waltham, MA, USA	Tris	10 % Goat normal serum	Supplemental figure S1
IgA	Rabbit	1:400	BETHYL laboratories, Montgomery, AL, USA	-	5 % Donkey normal serum	
IgG	Rabbit	1:400	BETHYL laboratories, Montgomery, AL, USA	-	5 % Donkey normal serum	
IgM	Rabbit	1:400	BETHYL laboratories, Montgomery, AL, USA	-	5 % Donkey normal serum	
C3	Rabbit	1:316	Abcam, Cambridge, UK	-	5 % Donkey normal serum	
Podocin	Rabbit	1:800	IBL, Gunma, Japan	CB	5 % Donkey normal serum	
Synaptopodin	Mouse	1:500	Fitzgerald Industries International, Acton, MA, USA	Tris	5 % Donkey normal serum	
WT-1	Rabbit	1:200	Santa Cruz Biotechnology, Dallas, TX, USA	CB	5 % Donkey normal serum	
Rabbit IgG-biotin	Goat	Undiluted	SABPO(R) Kit, Nichirei, Tokyo, Japan			Secondary antibody
Rat IgG-biotin	Goat	1:100	BioLegend, San Diego, CA, USA			
Rabbit IgG-Alexa Fluor 488	Donkey	1:500	Thermo Fisher Scientific, Waltham, MA, USA			
Rabbit IgG-Alexa Fluor546	Donkey	1:500	Thermo Fisher Scientific, Waltham, MA, USA			
Mouse IgG-Alexa Fluor 546	Donkey	1:500	Thermo Fisher Scientific, Waltham, MA, USA			
Rat IgG-Alexa Fluor 488	Donkey	1:500	Thermo Fisher Scientific, Waltham, MA, USA			

CASP3: Caspase 3, BrdU: Bromodeoxyuridine, FOXP3: Forkhead box P3, C3: Complement 3, WT-1: Wilms tumor 1 homolog, CB:10mM citrate buffer (pH 6.0), 115℃, 15 min. Tris: 20mM tris(hydroxymethyl)aminomethane-HCl (pH 9.0), 115℃, 15 min.

Supplementary Table S2. Primers used in this study.

Genes (Accession No.)	Primer Sequence (5'-3') F: Forward, R: Reverse	Product size (bp)
Casp1 NM_009807	F: GGTCTTGTGACTTGGAGGACA R: GGGTCACCCTATCAGCAGTG	96
Casp3 NM_009810	F: GGATCAAAGCGCAGTGTCCT R: CCCAGAGTCCACTGACTTGC	145
Casp4 NM_007609	F: CGATGTGGTGGTGAAAGAGGA R: CACCAGGAATGTGCTGTCTGA	106
Casp6 NM_	F: AGTGTCAGAGCCTGGTTGGA R: TGCGACAGAGTAGCACATGA	197
Casp7 NM_	F: CAACGACATTGACGCTAATCC R: GAGCATGGACACCATACACG	280
Casp8 NM_007609	F: CGATGTGGTGGTGAAAGAGGA R: CACCAGGAATGTGCTGTCTGA	106
Casp9 NM_001277932	F: GCGACATGATCGAGGATATTCAG R: CAGGAGATGAAGAGAGGAAGGG	118
Casp12 NM_009808	F: TAATGCTGACAGCTCCTCATGG R: TCCCTCCTTCTCCATCACTGG	134
Casp14 NM_009809	F: TGATCCTCAGCCATTGCAGG R: GGGATCCCTCTTCATGGTGC	163
Dffa NM_001025296	F: TTTGAGGATGGAGCTGTCGC R: TCCACTATGGTCCCGTCCTC	219
Fas NM_007987	F: CTGCAGACATGCTGTGGATCT R: TATCAGTTTCACGAACCCGCC	132
Bcl2 NM_009741	F: GAGTACCTGAACCGGCATCT R: GAGCAGGGTCTTCAGAGACAG	129
Bax NM_007527	F: ATCCAAGACCAGGGTGGCT R: GTGAGGACTCCAGCCACAAA	92
Rock1 NM_009071	F: CGGGCAAGAAGGTATCGTCA R: ACCAGGGCATCCAATCCATC	147
Il1b NM_008361	F: TTCCAGGATGAGGACATGAGC R: GACAAACTTCTGCCTGACGAG	111
Tnf NM_013693	F: TCTTCTCATTCCTGCTTGTGGC R: CATAGAACTGATGAGAGGGAGGC	119

Supplementary Figure S1. Phenotypes of mucosa-associated lymphoid tissues (MALT) in caspase 3 knockout mice.

For Supplementary figure S1a-c, to examine the proliferation in some mice, bromodeoxyuridine (BrdU) were intraperitoneal administrated at 100 mg/kg BW at 2 hours before sampling. The ileum including MALT was fixed with 4 % paraformaldehyde (PFA) at 4 ℃ overnight. The nasopharyngeal tissues including the bones were fixed with Bouin's solution for overnight and immersed in acetone overnight to eliminate lipid. Then, they were immersed in 10% formic acid for 4 hours to decalcify and washed with water.

For Supplementary figure S1, in the immunohistochemistry for BrdU (panels a, a', c, and c') and forkhead box P3 (FOXP3, panels a'', a''', c'', and c'''), the author selected some lymphoid clusters from ileum MALT (Peyer's patches) and nasopharynx. Furthermore, the area of lymphoid clusters and the number of positive cells were quantified by NDP. view2 (Hamamatsu Photonics Co., Ltd., Hamamatsu, Japan), and the positive cell number to examined area was calculated (panel b).

As a results, BrdU-incorporating cells or FOXP3-positive regulatory T-cells detected in the periphery of lymph nodes in Peyer's patches are not different between WT (panels a and a'') and KO mice (panels a' and a'''). Immunohistochemistry using females at 8 months. Bars = 200 μm. For measurement of the BrdU-incorporating cells or FOXP3-positive regulatory T-cells in lymph nodes in Peyer's patches using females at 8-12 months, there was no significant difference between WT and KO mice (panel b). Values are mean ± SE. Mann-Whitney *U*-test. For the nasopharyngeal tissues, there was no difference of the localization of these positive cells between WT and KO mice (panel c-c''').

Supplementary Figure S2. Glomerular pathology of caspase 3 knockout mice.

Glomerular features in caspase 3 knockout (KO) mice. Periodic acid-Schiff staining using mice at 6 months. There is no clear lesion in both sexes (panels a and a'). Bars = 50 μm.